HAL
open science

Retrofitting reinforced concrete structures with FRP: Numerical simulations using multifiber beam elements

Cédric Desprez, J. Mazars, Panagiotis Kotronis, Patrick Paultre, Nathalie Roy, Mathieu Boucher-Trudeau

To cite this version:

Cédric Desprez, J. Mazars, Panagiotis Kotronis, Patrick Paultre, Nathalie Roy, et al.. Retrofitting reinforced concrete structures with FRP: Numerical simulations using multifiber beam elements. ECCOMAS Thematic Conference on Computational Methods in Structural Dynamics and Earthquake Engineering (COMPDYN 2009), Jun 2009, Rhodes, Greece. hal-02369198

HAL Id: hal-02369198

https://hal.science/hal-02369198v1

Submitted on 18 Nov 2019

HAL is a multi-disciplinary open access archive for the deposit and dissemination of scientific research documents, whether they are published or not. The documents may come from teaching and research institutions in France or abroad, or from public or private research centers.

L'archive ouverte pluridisciplinaire **HAL**, est destinée au dépôt et à la diffusion de documents scientifiques de niveau recherche, publiés ou non, émanant des établissements d'enseignement et de recherche français ou étrangers, des laboratoires publics ou privés.

COMPDYN 2009
ECCOMAS Thematic Conference on
Computational Methods in Structural Dynamics and Earthquake Engineering
M. Papadrakakis, N.D. Lagaros, M. Fragiadakis (eds.)
Rhodes, Greece, 22-24 June 2009

RETROFITTING REINFORCED CONCRETE STRUCTURES WITH FRP: NUMERICAL SIMULATION USING MULTIFIBER BEAM ELEMENTS.

C. Desprez[1], J. Mazars[1], P. Kotronis[1],
P. Paultre[2], N. Roy[2] and M. B-Trudeau[2]

[1] Laboratoire Sols, Solides, Structures - Risques (3S-R), UJF/CNRS/INPG,
Domaine Universitaire, BP 53, 38041 Grenoble Cedex 9, France
e-mail: {Cedric.Desprez, Jacky.Mazars, Panagiotis.Kotronis}@hmg.inpg.fr

[2] Université de Sherbrooke, Faculté de génie, Département de génie civil,
2500 boulevard de l'Université, Sherbrooke, Québec J1K 2R1, Canada
e-mail: {Patrick.Paultre, Nathalie.Roy, mathieu.boucher-trudeau}@USherbrooke.ca

Keywords: FRP; confined concrete; reinforced concrete; numerical modeling; multifiber beam.

Abstract. *In structural engineering, seismic vulnerability reduction of existing structures is a crucial issue. External reinforcement by Polymer Reinforced Fibers (FRP) is an interesting tool in order to fulfill this aim. However, the use of FRP reinforcement as a retrofitting method is limited, one of the reasons being the lack of predicting numerical tools for cyclic loading.*

This paper presents a method to predict the behavior of beam-column structures considering the FRP reinforcement effect. It describes the construction of a $1D$ *concrete constitutive model suitable for monotonic and cycling loadings. The model is inspired on two well-known concrete models, the first one based on the damage mechanics theory (La Borderie concrete damage model), and the second one based on experimental studies (Eid & Paultre's confined concrete model). Validation of the approach is done using experimental results on reinforced concrete beam and columns submitted to axial and flexural cyclic loading. The proposed method deals also with steel bar rupture considering low cycle fatigue effects. All the simulations are done using multifiber Timoshenko beam elements.*

1 INTRODUCTION

Nowadays, Polymer Reinforced Fibers (FRP) are often used to retrofit existing buildings. This paper deals with a method to simulate their confinement effect in reinforced concrete (RC) structural elements using multifiber beams. We present the construction of a $1D$ concrete constitutive model suitable for monotonic and cycling loadings. The model is inspired on two well-known concrete models, the first one based on the damage mechanics theory (La Borderie concrete damage model), and the second one based on experimental studies (Eid & Paultre's confined concrete model). Comparisons with experimental results on RC beams and columns validate the approach.

2 MODELING TOOLS

2.1 Finite element discretisation

In order to decrease the number of degrees of freedom and thus to simplify the finite element mesh, Timoshenko multifiber beam elements are used to discretise the RC specimens [1],[2],[3]. Shear is considered linear, allowing using 1D constitutive laws (figure 1). All the calculations are done with FEDEASLab [4].

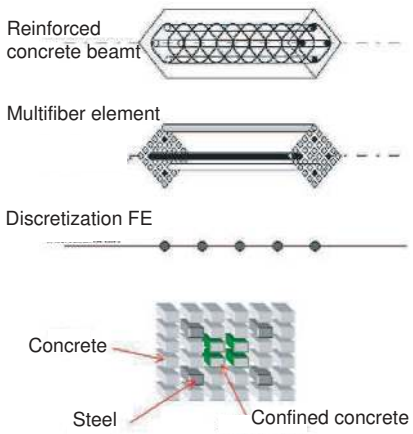

Figure 1: Multifiber beam modeling.

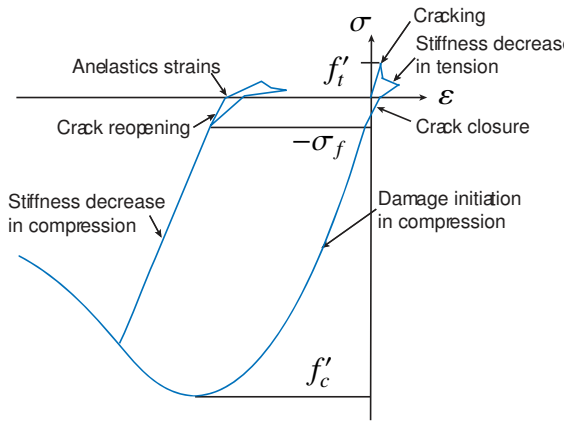

Figure 2: La Borderie cyclic model: uniaxial stress-strain relation.

2.2 Constitutive model for unconfined concrete under cyclic loading

A suitable constitutive model for (unconfined) concrete under cyclic loading is the one developed by C. La Borderie [5],[6]. Based on damage mechanics, it takes into account the opening and closing of cracks (figure 2). The general formulation of the model is tridimensional ($3D$), but only the uniaxial ($1D$) expression is used hereafter. Total strain (ε) is defined as the sum of an elastic (ε_e) and an anelastic part (ε_a) as follows:

$$\varepsilon = \varepsilon_e + \varepsilon_a \tag{1}$$

$$\varepsilon_e = \frac{\sigma^+}{E(1-D_1)} + \frac{\sigma^-}{E(1-D_2)} \tag{2}$$

$$\varepsilon_a = \frac{\beta_1 D_1}{E(1-D_1)} F'(\sigma) + \frac{\beta_2 D_2}{E(1-D_2)} \tag{3}$$

$$D_i = 1 - \frac{1}{1 + [A_i(Y_i - Y_{0i})]^{B_i}} \qquad \text{i=1 or 2} \tag{4}$$

σ^+ and σ^- are respectively the tensile and compressive stresses (eq. 5, 6); E is the initial Young's modulus of concrete; β_1 and β_2 are material constant parameters controlling the anelastic strains in tension and compression respectively; $F'(\sigma)$ is a function which controls the opening and closing of cracks (eq. 7, 8, 9); $-\sigma_f$ is the stress crack closure (figure 2); A_i and B_i are constants.

$$\sigma > 0 \;\rightarrow\; \sigma^+ = \sigma, \;\; \sigma^- = 0 \tag{5}$$

$$\sigma < 0 \;\rightarrow\; \sigma^+ = 0, \;\; \sigma^- = \sigma \tag{6}$$

$$\sigma \geq 0 \;\rightarrow\; F(\sigma) = \sigma \text{ and } F'(\sigma) = 1 \tag{7}$$

$$-\sigma_f \leq \sigma < 0 \;\rightarrow\; F(\sigma) = \sigma(1 + \frac{\sigma}{2\sigma_f}) \text{ and } F'(\sigma) = 1 + \frac{\sigma}{\sigma_f} \tag{8}$$

$$\sigma < -\sigma_f \;\rightarrow\; F(\sigma) = \frac{-\sigma_f}{2} \text{ and } F'(\sigma) = 0 \tag{9}$$

D_1 and D_2 (eq. 4) are the damage variables due to traction and compression respectively (varying from 0 (initial material) to 1 (damaged material)). D_i is piloted by Y_i (eq. 10, 11). Y_{0i} the initial damage threshold.

$$Y_1 = \frac{(\sigma^+)^2}{2E(1 - D_1)^2} + \frac{\beta_1.F(\sigma)}{E(1 - D_1)^2} \tag{10}$$

$$Y_2 = \frac{(\sigma^-)^2}{2E(1 - D_2)^2} + \frac{\beta_2.\sigma}{E(1 - D_2)^2} \tag{11}$$

2.3 Constitutive model for confined concrete under monotonic loading

A suitable $1D$ constitutive model for confined concrete under monotonic loading is the one developed by Eid & Paultre [7]. It is a global model taking into account internal (due to Transverse Shear Reinforcement TSR) and external (due to FRP) confinement, (see figure 3). The prepeak curve in the stress-strain relation is given by eq. 12, the postpeak relation before FRP failure by eq. 13 and the post-peak relation after FRP failure by eq. 14.

$$\sigma_c = \frac{a\varepsilon_c}{1 + b\varepsilon_c + z\varepsilon_c^2} \qquad \varepsilon_c \leq \varepsilon'_{cc} \tag{12}$$

$$\sigma_c = f'_{cc} exp\left[k_1(\varepsilon_c - \varepsilon'_{cc})^{k_2}\right] + E_{cu}(\varepsilon_c - \varepsilon'_{cc}) \qquad \varepsilon_{cu} > \varepsilon_c \geq \varepsilon'_{cc} \tag{13}$$

$$\sigma_c = f'_{cc,s} exp\left[k_{1,s}(\varepsilon_c - \varepsilon'_{cc,s})^{k_{2,s}}\right] \qquad \varepsilon_{\geq}\varepsilon_{cu} \tag{14}$$

σ_c and ε_c are the compressive axial stress and strain for the confined concrete; f'_c and ε'_c are the unconfined concrete cylinder compressive peak strength and strain; f'_{cc} and ε'_{cc} the compressive peak strength and strain of confined concrete (before FRP failure); $f'_{cc,s}$ and $\varepsilon'_{cc,s}$ the compressive peak strength and strain of steel-confined concrete (after FRP failure); f'_{cu} and ε'_{cu} the confined concrete cylinder compressive strength and strain at rupture; E_{cu} the slope of the axial stress-strain postpeak curve of concrete; a, b, and z are constants that control the initial slope and the curvature of the prepeak branch; k_1 and k_2 are parameters controlling the shape of the postpeak branch. The full setup of this model is presented in [7].

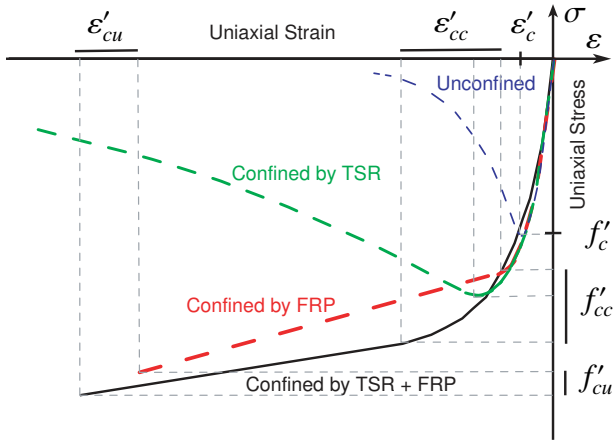

Figure 3: Eid & Paultre monotonic model: uniaxial stress-strain relation.

2.4 Constitutive model for steel and FRP reinforcement

- The cyclic behavior of steel reinforcement is simulated using the classical Menegotto-Pinto model [8], (figure 4).
- FRP is modeled considering an elastic brittle behavior in tension. Compression is neglected (figure 5).

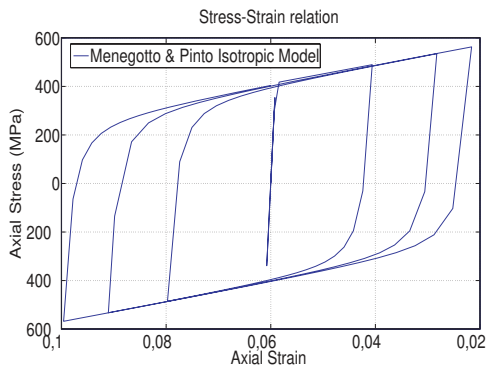

Figure 4: Menegotto-Pinto cyclic model: uniaxial stress-strain relation.

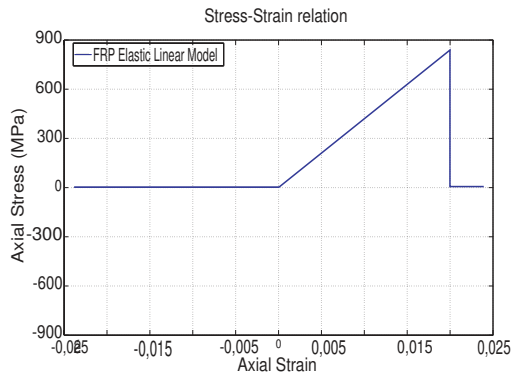

Figure 5: FRP elastic model: uniaxial stress-strain relation.

3 SIMULATING RC BEAMS RETROFFITED BY FRP

3.1 Principle of modeling

FRP reinforcement, bonded on one side of the beam (figure 6), has a function similar to the one of an external reinforcement bar. In a multifiber beam context, one can thus reproduce its contribution considering an additional fiber in the multifiber beam section (figure 7).

3.2 Experimental validation

3.2.1 Experimental set-up

The experimental results used to validate the proposed modeling strategy are based on the tests realized by G.Spadea & al [9] at the University of Calabre. Two beams are submitted

to a monotonic flexural load. The beams have the same geometry (figure 8), but only one is retrofitted by adding FRP on its lower part (figure 9). The load-deflection curves are provided.

Figure 6: Image of a RC beam retrofitted with FRP.

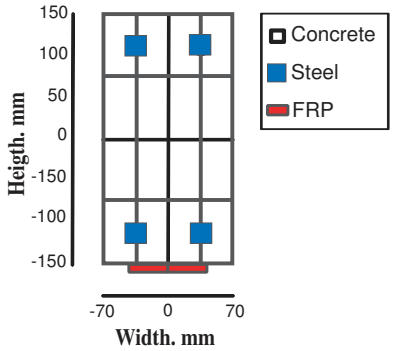

Figure 7: Additional steel and FRP fibers in the multifiber beam section.

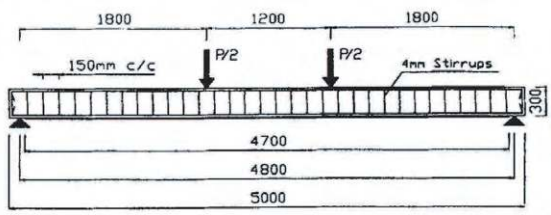

Figure 8: Geometrical characteristics of the beams.

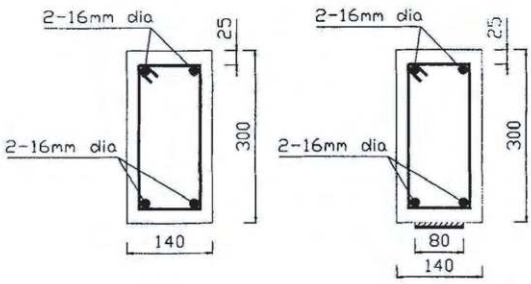

Figure 9: Normal and retrofitted beam section.

3.2.2 Multifiber discretization

The beam is discretized using 16 multifiber Timoshenko beam elements of 0.3m length. Each section is composed of 16 concrete fibers and 4 steel fibers. FRP is taken into account using 2 additional fibers at the bottom side of each section (figure 7).

The Young modulus of concrete and steel are assumed equal to 30 GPa and 200 GPa respectively. Other material parameters are taken from [9]. Perfect bonding is assumed between FRP and concrete (same strains at the interface).

3.2.3 Numerical versus experimental results

Numerical prediction results are close to the experimental data for the beam A3.3 (the beam with the better FRP sheet anchorage), (figures 10 and 11). The small increase of the stiffness in the first part of the curve (deflection <40mm) and the higher increase of the capacity later on (40<deflection<150mm) are accurately reproduced. The FRP failure for experimental A3.3 and numerical beams occurs for close deflection.

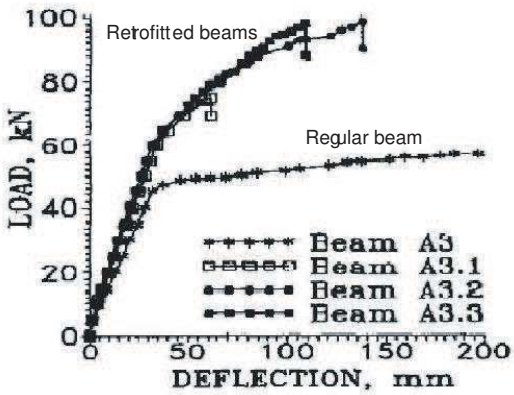

Figure 10: Experiments - Beams under flexion with and without FRP reinforcement: load vs deflection.

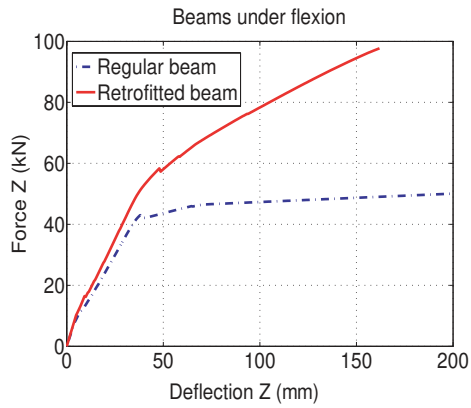

Figure 11: Simulations - Beams under flexion with and without FRP reinforcement: load vs deflection.

4 SIMULATING RC STRUCTURES RETROFFITED BY FRP

4.1 Principle of modeling

In structural concrete elements, the main mechanical effect of the internal and external confinement is to reduce the development of lateral expansions that cause the most part of the damage. In an uniaxial model based on damage mechanics theory, a simplified way to take this effect into account is to adapt the damage evolution law due to compression. The proposed strategy consists in adapting the damage evolution of the La Borderie model to fit the evolution proposed in Eid & Paultre's model [7]. This is done as follows:

In the uniaxial version of the La Borderie model, the axial strain takes the form

$$\varepsilon = \frac{\sigma^+}{E(1-D_1)} + \frac{\sigma^-}{E(1-D_2)} + \frac{\beta_1.D_1}{E(1-D_1)}F'(\sigma) + \frac{\beta_2.D_2}{E(1-D_2)} \tag{15}$$

Considering now the uniaxial monotonic compression ($\sigma = \sigma^-$), after crack closure ($F'(\sigma) = 0$), the relation in eq. 15 becomes:

$$\sigma = E.\varepsilon(1-D_2) - \beta_2 D_2 \tag{16}$$

Damage D_2 is thus calculated as:

$$D_2 = \frac{E.\varepsilon - \sigma}{E.\varepsilon + \beta_2} \tag{17}$$

Figures 12 and 13 represent the uniaxial stress stain curve in compression and the evolution of damage for the La Borderie and the Eid & Paultre models.

We can clearly see that confinement reduces the evolution of damage. The damage versus strain evolution is slower for confined than for unconfined concrete. We propose to replace the damage variable D_2 with a new variable D_{2c} calculated as follows:

$$D_{2c} = \frac{E.\varepsilon_c - \sigma_c}{E.\varepsilon_c + \beta_2} \tag{18}$$

Where σ_c is the axial stress in concrete computed from Eid & Paultre model (eqs. 12, 13 and 14). It is assumed that the unloading process and the behavior in traction are not affected by the confinement. The new uniaxial constitutive stress-strain relation (LMCC for La Borderie Modified for Confined Concrete) is presented in figure 14.

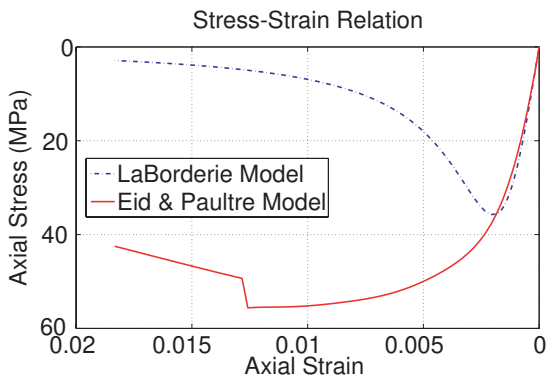

Figure 12: La Borderie and Eid & Paultre models: monotonic uniaxial stress strain curve in compression.

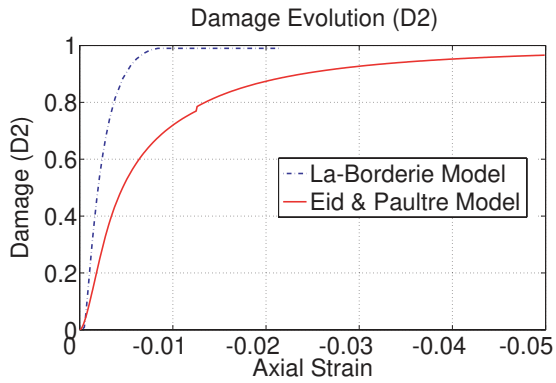

Figure 13: La Borderie and Eid & Paultre models: Damage evolution (D_2) due to compression.

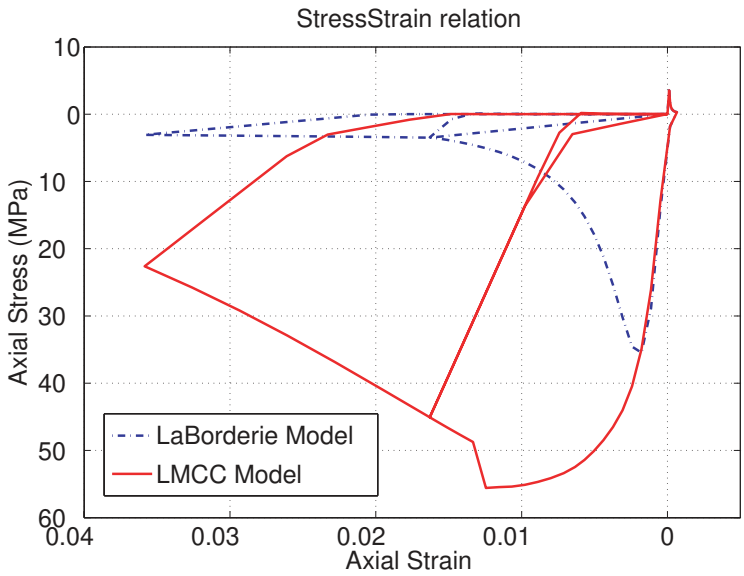

Figure 14: Cyclic behavior of the La Borderie model Modified for Confined Concrete (LMCC).

4.2 Experimental validation (1): RC columns under axial and flexural load

4.2.1 Experimental set-up

The experimental data used in this section come from tests on FRP reinforced concrete specimens performed at Sherbrooke University [10]. Two FRP confined ($P1$ and $P2$) and two unconfined ($P3$ and $P4$) RC cylindrical columns are submitted to axial and cyclic flexural loads (figures 15). The columns have the same geometrical characteristics (figures 16, 17). During the tests, the axial load is kept constant and equal to 10% ($P1$ and $P3$) or 35% ($P2$ and $P4$) of the estimated column capacity in uniaxial compression ($A_g f_c'$), (table 1). An horizontal cyclic displacement is applied at the top of each column till failure. A detailed description of the tests is available in [10].

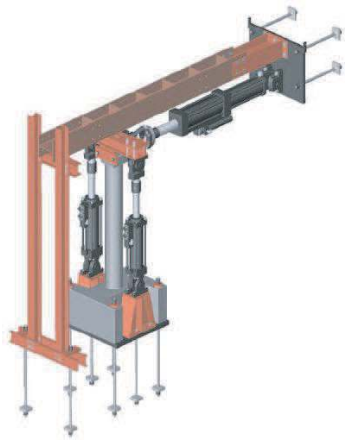

Figure 15: Experimental setup.

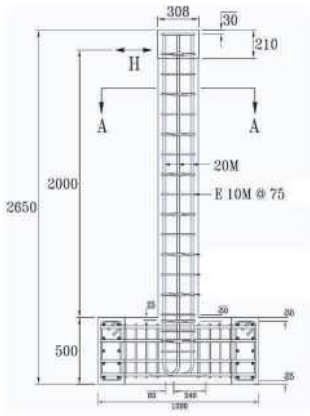

Figure 16: Geometrical characteristics of the columns.

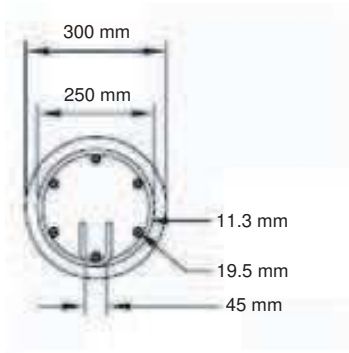

Figure 17: Section of the columns.

Test	FRP (mm)	Axial Load (KN)	% of capacity in compression
P1	1	224.3	10
P2	1	866.4	35
P3	0	234.3	10
P4	0	751.6	35

Table 1: Description of the tests.

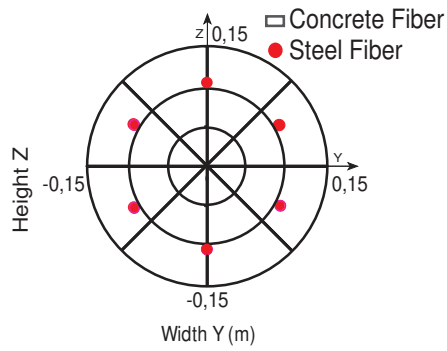

Figure 18: Location of the fibers in the multifiber beam section.

4.2.2 Multifiber discretization

Each column is reproduced using 5 multifiber Timoshenko beam elements. Each multifiber beam section contains 24 concrete fibers and 6 fibers for the longitudinal reinforcement steel bars (figure 18). It is assumed that the base of the column is fixed and its upper part is free. Material properties comes from experiments presented in [10].

4.2.3 Numerical versus experimental results

The significant gain in resistance and ductility due to the FRP confinement is correctly reproduced with the LMCC model (figures 19-22). The difference in the behavior of the confined and unconfined columns is clearly shown in figure 23. In this figure, we plot the stress-strain uniaxial relation in the same fiber for the confined (LMCC) and the unconfined (La Borderie) concrete (columns $P1$ and $P3$).

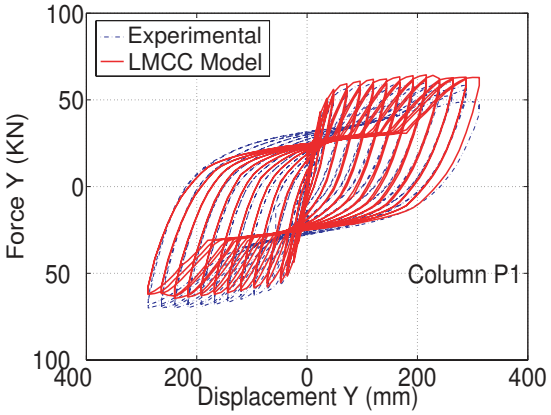

Figure 19: Confined column $P1$: computed results vs experimental data.

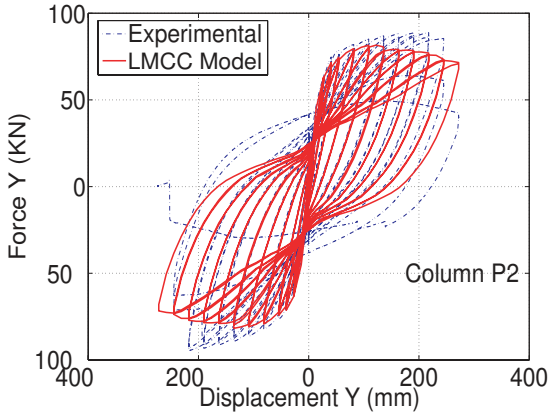

Figure 20: Confined column $P2$: computed results vs experimental data.

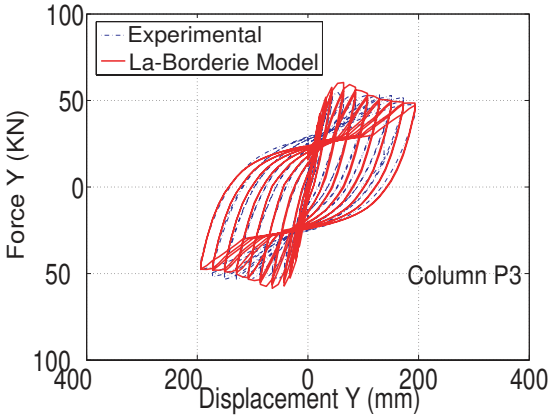

Figure 21: Unconfined column $P3$: computed results vs experimental data.

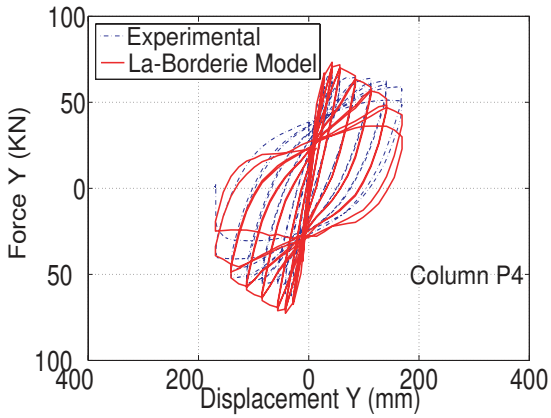

Figure 22: Unconfined column $P4$: computed results vs experimental data.

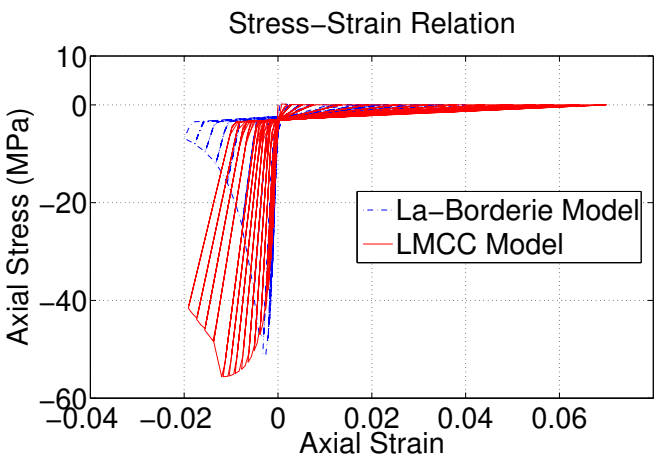

Figure 23: Axial stress-strain behavior in a concrete fiber for columns $P1$ and $P3$ (numerical results).

4.3 Experimental validation (2): Bridge pier under axial and flexural load

4.3.1 Experimental setting

A specimen representative of a bridge pier (1/3 scale) composed of 3 columns with partial retrofitting has recently been tested [10]. The bridge pier contains 3 identical columns of 2.1m height and a transverse beam. Only the two outer columns are retrofitted with FRP (the central column and the beam are not retrofitted). The axial load varies from 10% to 20% of $A_g f'_c$ (estimated column capacity in uniaxial compression) during the cycles. The lateral imposed displacement is cyclic with increasing intensity. During the test, the force-displacement curve is measured.

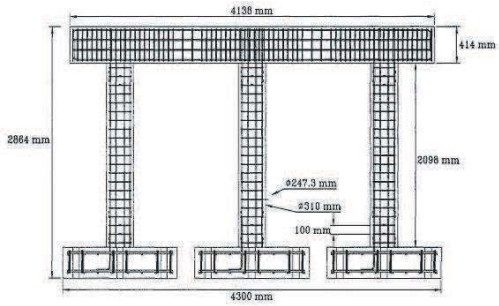

Figure 24: Bridge pier geometrical characteristics.

Figure 25: Retrofitted and not retrofitted columns.

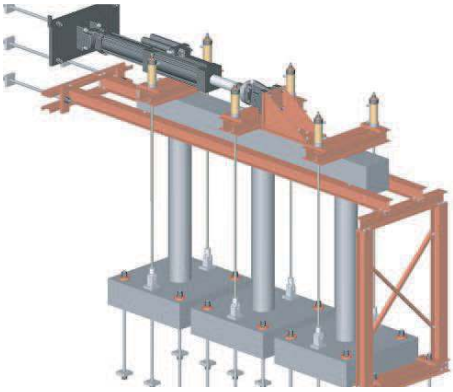

Figure 26: Bridge pier experimental setup.

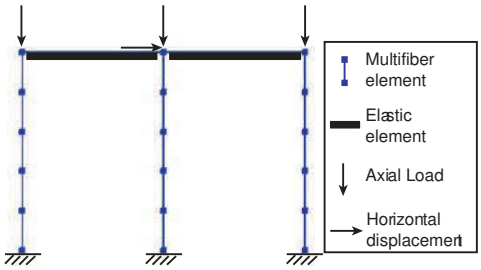

Figure 27: Bridge pier numerical modeling.

4.3.2 Multifiber discretization

Each column is modeled using 5 Timoshenko multifiber elements (figure 27). Columns are considered fixed at the bottom. The transverse beam is assumed elastic with a reduced section to take into account the initial cracks in the concrete. Each multifiber section contains 24 concrete fibers and 15 fibers representing the longitudinal steel bars. Material parameters are based on experimental tests [11]. Two numerical simulations are presented hereafter:

- The first numerical test ($N1$) reproduces the behavior of the bridge without considering FRP effects. Results are compared with the experimental data of the retrofitted bridge in order to quantify the FRP influence. The material model used for the three columns is the classical La Borderie model (without any modification). Steel is modeled using the Menegotto-Pinto model.

- The second numerical test ($N2$) considers a retrofitted model for the bridge. Comparison with the experimental data shows the performance of the proposed modeling strategy. The material model used for the unconfined concrete (central column) is the La Borderie model; for the confined concrete (outer columns) the LMCC model and for the steel bars the Menegotto-Pinto model.

4.3.3 Numerical versus experimental results

- Figure 28 shows that the experimental peak strength of the retrofitted bridge pier is 20% higher of the strength computed without retrofitting ($N1$).
- Figure 29 shows that the LMCC model is able to reproduce the FRP effect ($N2$). Predictions are close to the experimental data especially during the first part of the test (before collapse).

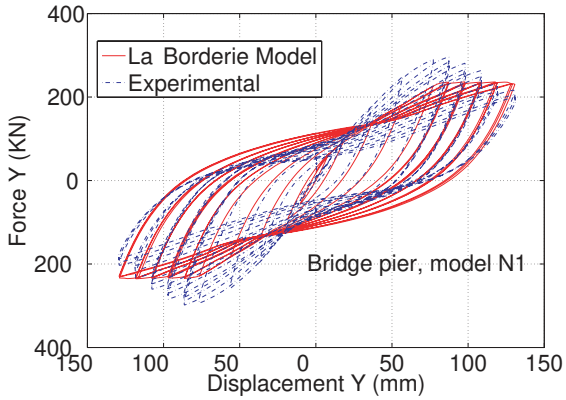

Figure 28: Bridge pier specimen: comparison between experimental and numerical data without considering FRP ($N1$ simulation).

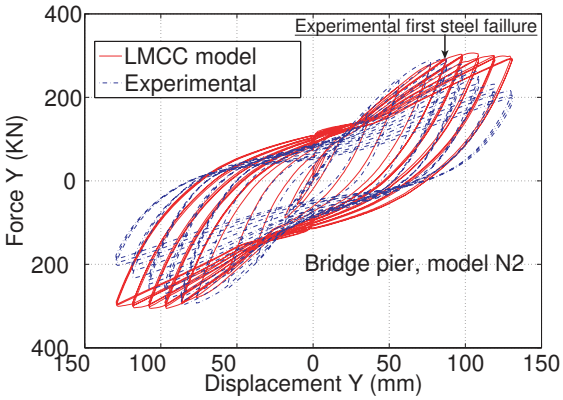

Figure 29: Bridge pier specimen: comparison between experimental and numerical data considering FRP ($N2$ simulation).

In the following section, we show that in order to reproduce correctly the whole experiment one has to take into account the low cycle fatigue in the reinforced steel bars.

5 LOW CYCLE FATIGUE IN REINFORCED STEEL BARS

The lack of information about the low cycle fatigue in steel may cause an overestimation of the structure capacity (see figure 29). This section presents a simplified way to take this phenomenon into account.

5.1 Principle of modeling

Based on the well known Miner's theory [12], the proposed strategy consists in the evaluation of low cycle fatigue in steel considering a damage index D_S. This index is a function of the strain cycles in the steel. In other words, it is assumed that above a strain amplitude threshold, every new cycle i increases the damage index D_S. D_S can only increase and it varies from 0 (initial steel bar) to 1 (broken steel bar). According to [12], D_S is calculated as:

$$D_S = \sum_{i=1}^{n} D_{Si} \tag{19}$$

$$D_{Si} = \frac{1}{N_{ri}} \tag{20}$$

$$N_{ri} = \frac{C_S^2}{\Delta\varepsilon^2} \tag{21}$$

D_{Si} is the damage value caused by the cycle i; N_{ri} is the maximal number of cycles at failure done at the same strain amplitude $\Delta\varepsilon$; C_S is a material constant computed by the widely used fatigue life model of Coffin & Manson [13][14].

5.1.1 Experimental validation: Bridge pier under axial and flexural load

The previous method is applied for the numerical analysis of the retrofitted bridge. The strain history of each steel fiber is used to calculate its damage index D_S. As we can see in figure 30, D_S starts increasing from a given strain threshold. For the specific steel fiber in figure 30, D_S reaches 1 just one cycle before the steel bar broke experimentally. As shown in figure 32, the introduction of the low cycle fatigue in steel allows improving the performance of numerical simulation of the bridge pier even for the ultimate stages of the experiment.

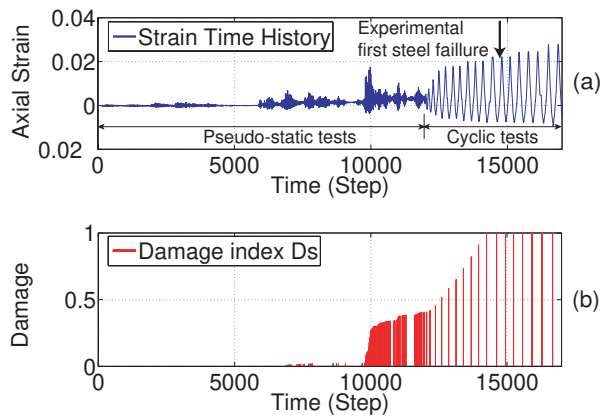

Figure 30: (a) Axial strain-time history in a steel fiber, (b) Evolution of the damage index D_S in the fiber.

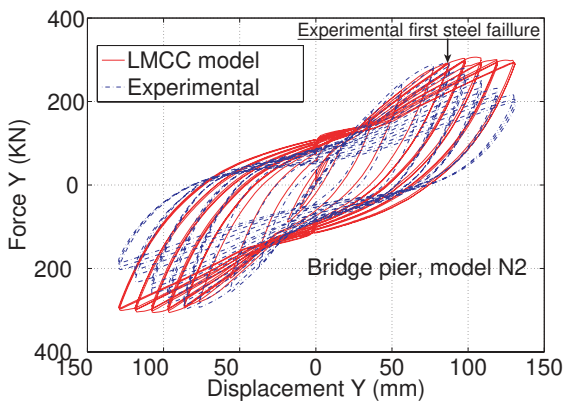

Figure 31: N2, Bridge pier specimen: comparison between experimental and numerical data without considering the low cycle fatigue in steel ($N2$ simulation).

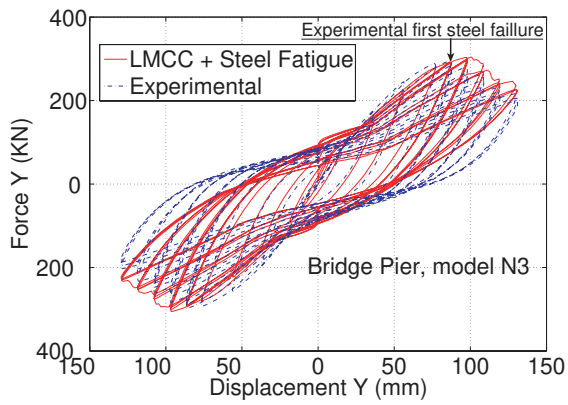

Figure 32: N3, Bridge pier specimen: comparison between experimental and numerical data considering the low cycle fatigue in steel ($N3$ simulation).

6 CONCLUSION

In this work, simplified modeling strategies to reproduce the non linear cyclic behavior of retrofitted with FRP RC structures were presented. More specifically:

- Spatial discretization is done using multifiber beam elements.
- A modification of the La Borderie model is proposed based on the Eid & Paultre confined concrete model.
- Low cycle fatigue in steel is introduced using Miner's theory.
- Validation is provided using experimental results on RC beams, columns and bridge piers.

The methods developed in this paper can serve as simplified tools to do comparative studies on the vulnerability of structures before and after FRP retrofitting.

REFERENCES

[1] Kotronis P. and Mazars J. Simplified modelling strategies to simulate the dynamic behaviour of R/C walls. Journal of Earthquake Engineering, 9(2), 285–306, 2005.

[2] Mazars J., Kotronis P., Ragueneau F., and Casaux G. Using multifiber beams to account for shear and torsion : Applications to concrete structural elements. Computer Methods in Applied Mechanics and Engineering, 195(52), 7264–7281, 2006.

[3] Kotronis P. Stratégies de modélisation de structures en béton soumises à des chargements sévères. Habilitation à diriger des recherches, http://tel.archives-ouvertes.fr/tel-00350461/fr/, Université Joseph Fourier, 2008.

[4] Filippou F. and Constandines M. Fedeaslab getting started guide and simulations examples. Dpt of civil and env. Engng. UC Berkeley, 2004.

[5] La Borderie C. Phénomènes unilatéraux dans un matériau endommageable: Modélisation et application à l'analyse des structures en béton. Thèse de doctorat, Université Paris VI, Paris, France, 1991.

[6] La Borderie C. Stratégies et modèles de calculs pour les structures en béton. Habilitation à diriger des recherches, Université de Pau et des Pays de l'Adour, France, 2003.

[7] Eid R. and Paultre P. Analytical model for FRP-confined circular reinforced concrete columns. Journal of Composites for Construction, 12(5), 541–552, 2008.

[8] Menegotto M. and Pinto P. Method of analysis of cyclically loaded reinforced concrete plane frames including changes in geometry and non-elastic behaviour of elements under combined normal force and bending. IABSE Symposium on resistance and ultimate deformability of structures acted on by well-defined repeated loads, final report, Lisbon, 1973.

[9] Spadea G., Bencardino F., and Swamy R. Structural behavior of composite RC beams with externally bonded CFRP. J. Compos. for Constr, 2(3), 132–137, 1998.

[10] Trudeau M., Tavares D., Roy N., and Paultre P. Centre de Recherche en Génie Parasismique et en Dynamique des Structures (CRGP), Université de Sherbrooke, Works in progress, 2008.

[11] Roy N. Réhabilitation parasismique performantielle des ponts avec des polymères renforcés de fibres de carbone. Thèse de doctorat, Université de Sherbrooke, 2006.

[12] Miner M. Cumulative damage in fatigue. Journal of applied mechanics, 67, A159–A154, 1945.

[13] Coffin L. A study of the effects of cyclic thermal stresses on ductile metal. Transactions of ASME, 76, 931–950, 1954.

[14] Manson S. Behaviour of materials under conditions of thermal stress. NACA report 1170, Lewis Flight Propulsion Laboratory, Cleveland, USA, 1954.